

Enhancing mechanical properties of an Mg–Zn–Ca alloy via extrusion

Yuzhou Du, Wei Du, Danli Zhang, Yanfeng Ge & Bailing Jiang

To cite this article: Yuzhou Du, Wei Du, Danli Zhang, Yanfeng Ge & Bailing Jiang (2021) Enhancing mechanical properties of an Mg–Zn–Ca alloy via extrusion, Materials Science and Technology, 37:6, 624-631, DOI: [10.1080/02670836.2021.1938861](https://doi.org/10.1080/02670836.2021.1938861)

To link to this article: <https://doi.org/10.1080/02670836.2021.1938861>



Published online: 14 Jun 2021.



Submit your article to this journal [↗](#)



Article views: 129



View related articles [↗](#)



View Crossmark data [↗](#)



Citing articles: 1 View citing articles [↗](#)



Enhancing mechanical properties of an Mg–Zn–Ca alloy via extrusion

Yuzhou Du^{a,b}, Wei Du^a, Danli Zhang^c, Yanfeng Ge^{a,b} and Bailing Jiang^{a,b}

^aSchool of Materials Science and Engineering, Xi'an University of Technology, Xi'an, People's Republic of China; ^bShaanxi Province Engineering Research Center for Magnesium Alloys, Xi'an University of Technology, Xi'an, People's Republic of China; ^cSchool of Materials Science and Engineering, Xi'an Jiaotong University, Xi'an, People's Republic of China

ABSTRACT

The mechanical properties of an Mg–Zn–Ca alloy were significantly improved through extrusion deformation. High-density spheroidal $\text{Ca}_2\text{Mg}_6\text{Zn}_3$ with a diameter ranging from 10 to 50 nm dynamically precipitated during extrusion deformation. The microstructure of the as-extruded alloy was obviously refined compared with that of the as-cast counterpart. A bimodal microstructure consisting of coarsely deformed grains and finely recrystallised grains was obtained through extrusion. Additionally, the as-extruded alloy exhibited a strong basal texture. Consequently, the yield strength increased from 42 MPa of the as-cast alloy to 285 MPa of the as-extruded alloy.

ARTICLE HISTORY

Received 19 January 2021
Revised 26 May 2021
Accepted 1 June 2021

KEYWORDS

Mg–Zn–Ca; extrusion; recrystallisation; dynamic precipitation; mechanical properties

Introduction

Mg alloys are desirable candidates in fields requiring light weight because of their low density and high specific strength [1,2]. However, Mg alloys with low strength compared with their competitive Al alloys strongly restrict their applications. Hence, it is necessary to optimise the microstructure to enhance the mechanical properties of Mg alloys [3].

The mechanical properties of Mg alloys can be enhanced via the addition of a large concentration of alloying elements [4,5] and the thermomechanical process [6, 7]. A tensile yield strength of 360 MPa was achieved for an Mg–8.8Sn–4.0Zn–0.9Al–0.3Na (wt-%) alloy after extrusion and aging treatment [8], while an Mg–5.5Al–3Ca–0.3Mn (wt-%) alloy with a yield strength of 402 MPa was obtained through extrusion deformation [9]. However, an Mg alloy with high concentrations of alloying elements forms a coarse second phase and deteriorates the formability of Mg alloys. Therefore, solution treatment is commonly adopted to reduce the amounts of second phase in Mg alloys before deformation [10]. For example, an Mg–7.50Al–1.07Ca–0.17Mn (wt-%) alloy was solutionised at high temperature, which promoted the dissolution of the second phase and improved the room temperature stretch formability [10]. Recently, dilute Mg alloys with small amounts of alloying elements were proposed because of their superior formability and mechanical properties [11–15]. For instance, an Mg–0.31Al–0.3Ca–0.8Mn (wt-%) alloy could be extruded at a high die-exit speed of

60 m min⁻¹ without surface cracks [15], and a dilute Mg–0.21Zn–0.30Ca–0.14Mn (wt-%) alloy showed a tensile yield strength of 307 MPa after extrusion [16]. Therefore, low-alloyed Mg alloys might be an effective path for the future [10].

Mg–Zn–Ca-based alloys are suggested to be a promising Mg alloys series because of low price [17] and high biocompatibility. Previous investigations focused on Mg–Zn–Ca alloys with high amounts of Zn to improve strength through the generation of high-density precipitates during deformation [18,19]. For example, Mg–6Zn–0.8Ca (wt-%) with an ultimate tensile strength (UTS) greater than 300 MPa had been developed through extrusion deformation [20,21]. It should be noted that high Zn content in Mg–Zn–Ca alloys reduced the plasticity and increased the susceptibility of hot tearing [22]. Hence, reducing Zn content in Mg–Zn–Ca alloys was required to satisfy the manufacturing demands. Mg–1Zn–xCa alloys exhibited an ultimate strength less than 250 MPa [23] because an effective strengthening phase was not introduced when Zn content was low. Additionally, Ca is commonly added in limited amounts in Mg alloys because Ca shows low solubility in Mg and higher concentrations of Ca in the Mg alloy would form a stable second phase and deteriorate the formability.

Based on the above observations, an Mg–Zn–Ca alloy with about 2 wt-% Zn and about 0.1 wt-% Ca was fabricated and extruded in the present study, to achieve balanced strength and ductility of the Mg–Zn–Ca alloy.

Experimental procedure

Commercial high-purity Mg (99.9%, mass fraction), Zn (99.9%) and Mg–15%Ca master alloys were melted at 750°C in an electric resistance furnace under a mixed atmosphere of CO₂ and SF₆. The melts were held at 750°C for 10 min to ensure a homogeneous mixture. Then the temperature was decreased to 720°C and held for 10 min. After that, the melts were poured into a steel mould, which was preheated to 200°C. The alloy composition was analysed using an inductively coupled plasma (ICP) analyzer, and the result was shown to be Mg–1.876Zn–0.112Ca (wt-%). The casting ingots were cut into a rod with a diameter of 60 mm and a height of 40 mm. Then the rods were homogenised at 400°C for 10 h. After that, extrusion was conducted at 350°C with an extrusion ratio of 16 and an extrusion speed of about 10 mm min⁻¹. The extruded profile was cooled to ambient temperature in air.

The specimens for optical microscopy (OM) and scanning electron microscope (SEM) observation were first mechanically ground and polished and then etched using acetic picral. The phase constituents of the as-cast sample were determined by X-ray diffraction. The samples for electron backscatter diffraction (EBSD) observation were electro-polished in a solution of 62.5% ethanol and 37.5% orthophosphoric acid with an electric current of 0.1–0.5 A for 10–60 s at a temperature less than 20°C. EBSD was conducted on a Quanta 200 FEG device equipped with an EBSD detector. The obtained orientation data were recalculated to acquire pole figures with the MTEX 5.5.1 toolbox [24]. TEM specimens were ion-milled to perforation at an ion accelerating voltage of 3 kV. Microstructure characterisation was carried out on a Tecnai G2 F30 transmission electron microscope (TEM).

The as-extruded alloys were machined into a gauge length of 15 mm and cross-sectional area of 6 mm × 2 mm. Tensile tests were conducted using an Instron 5569 universal test machine at a crosshead speed of 1 mm min⁻¹ at ambient temperature. At least three samples were measured to ensure reproducibility.

Results

Figure 1 shows the dendritic microstructure of the as-cast alloy (Figure 1(a)). The backscattered electron (BSE) image of the as-cast alloy is shown in Figure 1(b). It could be clearly seen that the second phase with bright contrast was mainly distributed between dendrites. Additionally, the boundaries between dendrites with bright contrast could be observed, indicating that Zn or Ca elements were distributed inhomogeneously around the Mg matrix. EDS results of the second phase in Figure 1(b) demonstrated Mg, Ca and Zn concentrations. Previous investigations suggested that the second phases in Mg–Zn–Ca alloys

are Mg₂Ca and Ca₂Mg₆Zn₃ [25]. The type of second phase was determined by the atomic ratio of Zn and Ca in Mg–Zn–Ca alloys [26], where Ca₂Mg₆Zn₃ was the predominant phase when the value of Zn/Ca was greater than 1.23 [26]. The atomic ratio of Zn and Ca in Mg–1.88Zn–0.13Ca (wt-%) was about 8.9. Hence, it was inferred that the second phase should be Ca₂Mg₆Zn₃. Figure 1(d) presents the XRD patterns of the as-cast alloy. It could be seen that the peaks corresponding to the Ca₂Mg₆Zn₃ phase with low intensity appeared along with the Mg peaks. The low intensity of the Ca₂Mg₆Zn₃ peaks indicated that the amounts of Ca₂Mg₆Zn₃ were small.

To further confirm the second phase in the as-cast alloy, selected area electron diffraction (SAED) was conducted, which is shown in Figure 2. The diffraction pattern could be indexed by Ca₂Mg₆Zn₃, which confirmed that the second phase in the as-cast alloy was Ca₂Mg₆Zn₃.

Figure 3 shows the microstructure of the as-homogenised and as-extruded samples. It could be seen that the as-homogenised sample exhibited a coarse microstructure with dendritic morphology. Almost no second phase was detected in the as-homogenised alloy (Figure 3(a)), indicating that the second phase was dissolved into the matrix during homogenisation. After extrusion, the microstructure obviously changed. A bimodal microstructure consisting of coarsely deformed grains and finely directly recrystallised grains (DRGs) were observed (Figure 3(a)). The volume fraction of the DRG was estimated to be about 63%, and the size of DRG was about 2 μm. The microstructure of the as-extruded sample (Figure 3(b)) was much finer than that of the as-cast sample (Figure 3(a)).

Figure 4 shows the SEM images of the as-extruded alloy. Some tiny spheroidal precipitates were observed at the grain boundary and grain interior, which suggested that dynamic precipitation occurred during extrusion.

Figure 5 shows the TEM images of the as-extruded alloy. High-density dislocation and spheroidal precipitates in the deformed grains (Figure 5(a)) were detected. Fine precipitates with diameters ranging from 20 to 50 nm were distributed at grain boundaries and grain interiors (Figure 5(b)). To further confirm the type of precipitates in the as-extruded alloy, a high-resolution TEM (HRTEM) image of the precipitate is presented in Figure 5(c). The corresponding fast Fourier transform (FFT) of the precipitate is shown in Figure 5(d), which was indexed by Ca₂Mg₆Zn₃. It indicated that the dynamically spheroidal precipitates in the present alloy were Ca₂Mg₆Zn₃.

Figure 6 shows the EBSD maps of the as-extruded alloy, and the corresponding pole figures of the as-extruded alloy were presented. DRGs and deformed recrystallised grains were clearly observed. However,

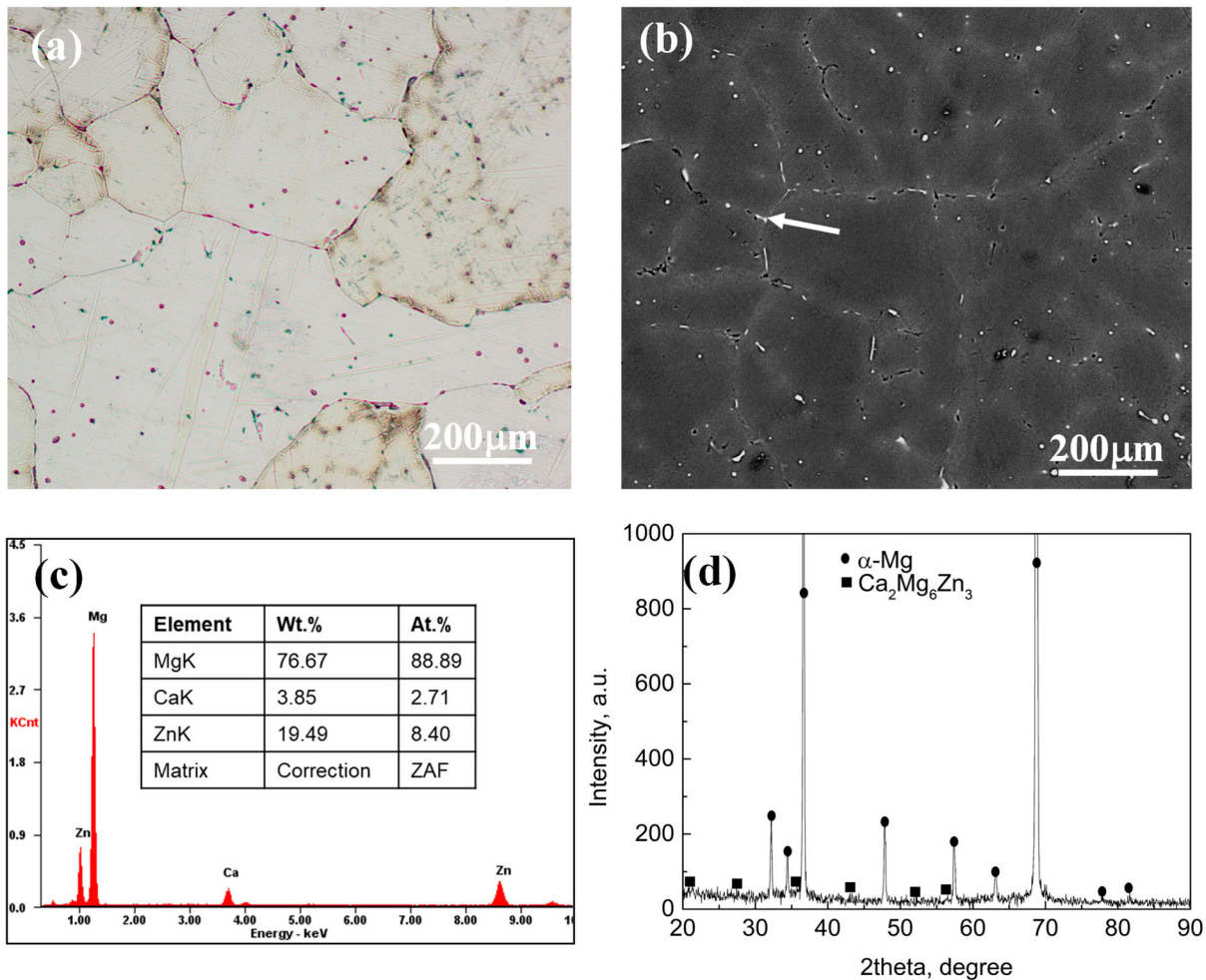


Figure 1. (a) optical and (b) BSE image of the as-cast alloy, (c) EDS of the second phase arrowed in b, (d) XRD patterns of the as-cast alloy.

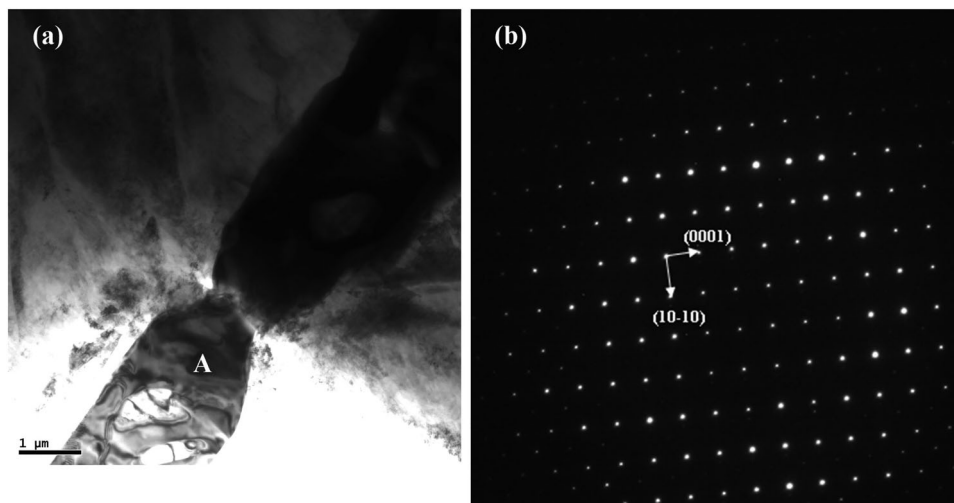


Figure 2. (a) Bright-field TEM image and (b) corresponding selected area electron diffraction pattern of the second phase A.

the orientations represented by colour obviously differed. The deformed grains with green colour suggested the $\langle 11\text{-}20 \rangle$ oriented grains, while the DRGs exhibited different colours, indicating more random orientations (Figure 6(a)). A strong basal texture with basal planes oriented towards extrusion

direction was obtained for the as-extruded alloy (Figure 6(b)), which was usually observed for wrought Mg alloys [27]. This strong texture is an important factor causing increased strength of the as-extruded Mg–Zn–Ca alloy, which will be discussed in the following.

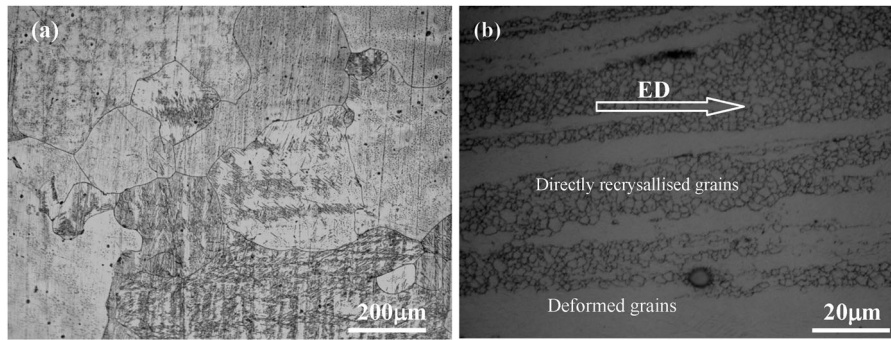


Figure 3. Optical images of the (a) as-homogenised and (b) as-extruded alloy.

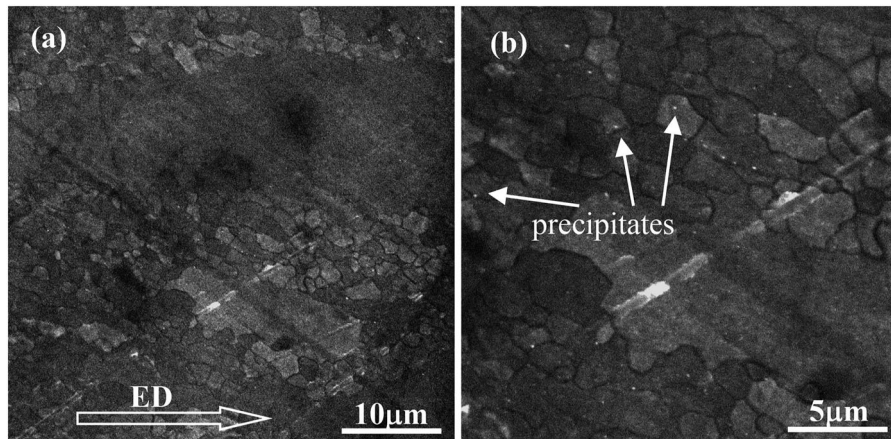


Figure 4. SEM images of the as-extruded alloy with (a) low and high magnifications.

Figure 7 shows the typical stress–strain curves of the Mg–Zn–Ca alloy. It could be seen that the yield strength (YS), UTS and elongation of the as-cast alloy were 42 ± 2 MPa, 135 ± 1 MPa, $6.1 \pm 0.2\%$, respectively. After homogenisation, the yield strength was similar to that of the as-cast alloy, but the elongation was increased to $8.2 \pm 0.2\%$. For the as-extruded sample, the YS was increased to 285 ± 3 MPa, the UTS was increased to 304 ± 3 MPa and the elongation was increased to $9.1 \pm 1.0\%$. This suggested that extrusion deformation enhanced the strength and ductility of the Mg–Zn–Ca alloy simultaneously.

Discussion

Extrusion effectively refined the microstructure, promoted dynamic precipitation of Mg–Zn–Ca alloy and enhanced the mechanical properties. The microstructure evolution and strengthening mechanism are discussed in the following.

Microstructure evolution of Mg–Zn–Ca alloy during extrusion

At the initial stage of extrusion, the initial grain was elongated along the extrusion direction accompanied with grain boundaries along the extrusion direction. Recrystallised grains preferentially nucleated at grain

boundaries. With the deformation proceeding, the recrystallised region was increased while the region further from the grain boundaries remained as deformed grains. Consequently, a microstructure with finely recrystallised grains and deformed grains was alternatively distributed. Accompanying the dynamic recrystallisation, dynamic precipitation also occurred. The initial $\text{Ca}_2\text{Mg}_6\text{Zn}_3$ phase in the as-cast alloy was dissolved into the matrix during homogenisation treatment (Figure 3(a)), which resulted in the supersaturation of Zn and Ca in Mg matrix. During extrusion, Ca and Zn tend to precipitate outside of the matrix. Additionally, extrusion resulted in increased dislocation, which could further promote dynamic precipitation. On the other hand, the low mixture entropy between Zn and Ca [28] was beneficial for the formation of Ca–Zn clusters [29], which had been detected in the Mg–Zn–Ca alloy [28]. These Ca–Zn clusters induce nucleation of the precipitate. Consequently, the as-extruded Mg–Zn–Ca alloy exhibited densely fine precipitates.

Figure 8 presents the microstructural evolution of the Mg–Zn–Ca alloy during hot extrusion. The as-homogenised alloy exhibited a coarse microstructure (Figure 8(a)). At the initial deformation, the initial grains were deformed and elongated along the extrusion direction. Grain boundaries were the preferential sites for recrystallised nucleation (Figure 8(b)),

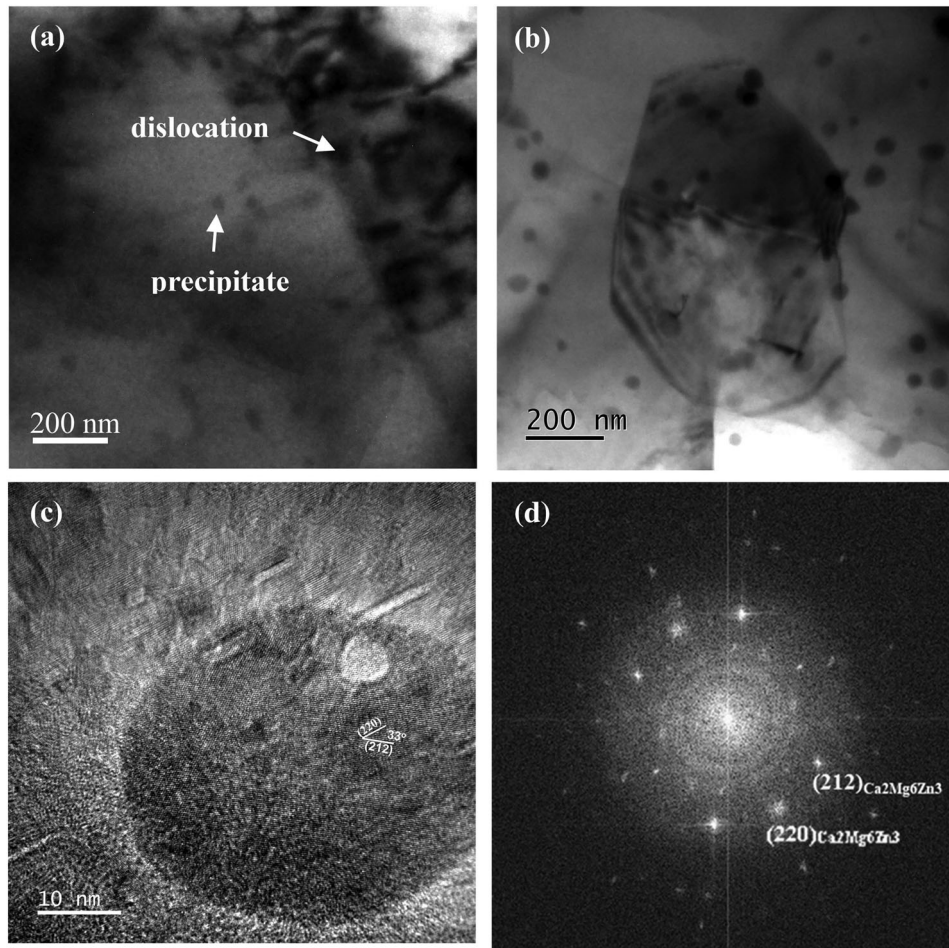


Figure 5. TEM bright filed (BF) images in (a) deformed grains and (b) directly recrystallised grains; (c) HRTEM image of precipitate and (d) corresponding FFT of the spherical precipitate.

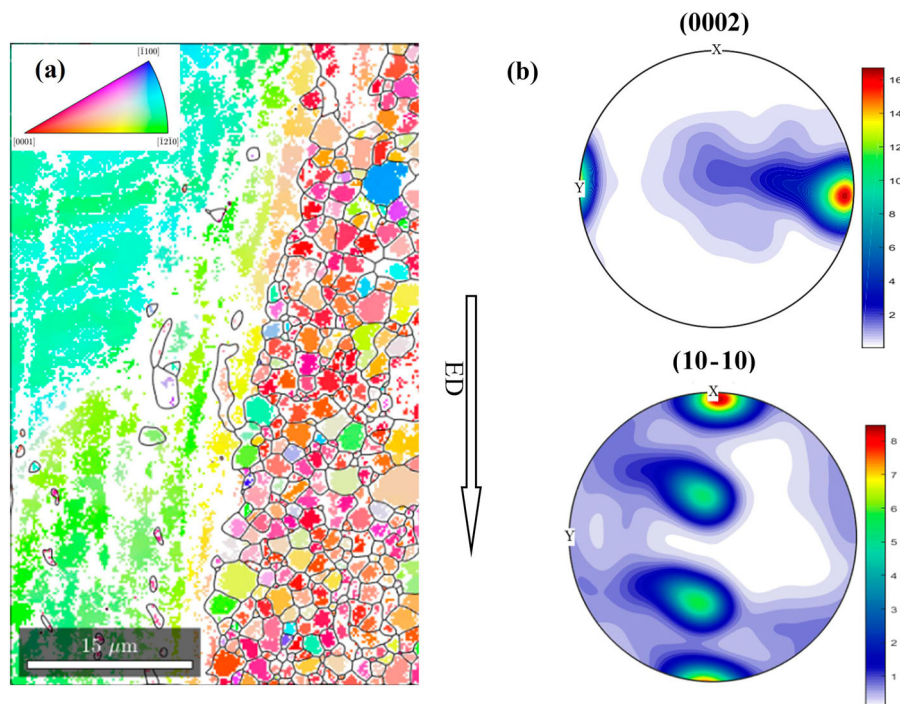


Figure 6. (a) EBSD map and corresponding (b) pole figures.

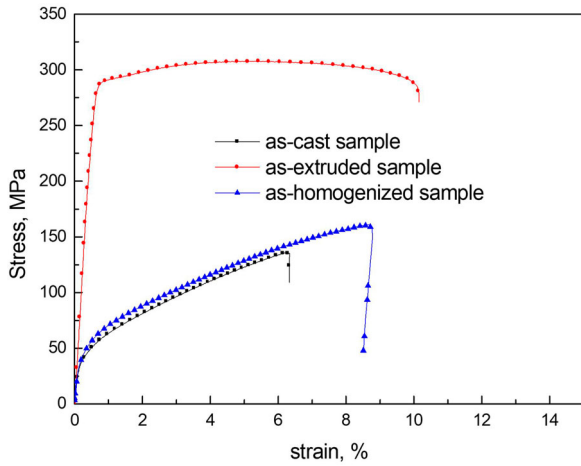


Figure 7. Typical stress–strain curves for the Mg–1.88Zn–0.13Ca (wt-%) alloy measured at ambient temperature.

which resulted in the formation of finely recrystallised grains. Additionally, fine $\text{Ca}_2\text{Mg}_6\text{Zn}_3$ precipitates were dynamically precipitated at the matrix because of the supersaturated Zn and Ca in Mg matrix. With further deformation, the initial grains were further elongated along the extrusion direction, and $\text{Ca}_2\text{Mg}_6\text{Zn}_3$ at grain boundaries prohibited the growth of recrystallised grains and that at the deformed grains hindered dislocation mobility. Consequently, the region away from the grain boundaries contained high-density dislocation.

Strengthening mechanism

Balanced mechanical property with a yield strength of 285 MPa and elongation of 9.1% were obtained for the as-extruded Mg–Zn–Ca alloy (Figure 7). Extrusion deformation effectively improves the mechanical properties of Mg–Zn–Ca alloy. The as-extruded alloy contained finely recrystallised grains, coarsely deformed grains with high-density dislocation, fine precipitates and strong basal texture. Hence, the improved mechanical properties of the as-extruded alloy are attributed to grain boundary strengthening in recrystallised grains and precipitate strengthening and texture strengthening in both regions.

The Hall–Petch relationship $\Delta\sigma_{\text{gb}} = kd^{-1/2}$, where k is the slope and d is the grain size, was commonly

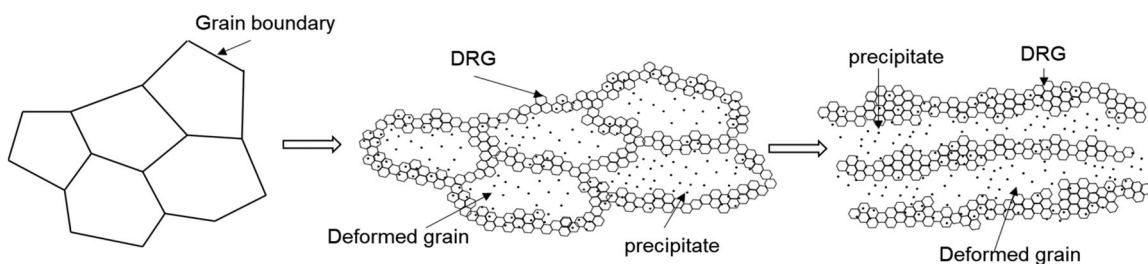


Figure 8. The schematic diagram of the microstructure evolution during extrusion of the Mg–Zn–Ca alloy.

employed to explain the grain boundary strengthening. The value of $k = 217 \text{ MPa } \mu\text{m}^{1/2}$ was previously reported for Mg–Zn-based alloys [30]. The average grain size for the DRG of the as-extruded sample was about $2 \mu\text{m}$ (Figure 3), which is much smaller than that of the as-cast and as-homogenised samples although it is difficult to accurately estimate the grain size of the as-cast and homogenised samples. Therefore, the contribution of grain size of DRG to strength was estimated to be about 153 MPa.

The dense $\text{Ca}_2\text{Mg}_6\text{Zn}_3$ phase and strong basal texture of the as-extruded Mg–Zn–Ca alloy are the other important factors causing the increased strength. The fine precipitates at grain boundaries and grain interior could inhibit the movement of dislocations during tensile deformation. The enhanced strength due to precipitates was determined by the size and spacing of the precipitates according to Orowan–Ashby theory [31]. The average diameter of the precipitates in the as-extruded Mg–Zn–Ca alloy was about 30 nm and the spacing was about 80 nm (Figure 4). Then the incremental shear strength for the activation of basal slip could be inferred to be about 54 MPa. Owing to the basal texture formed after extrusion, the Schmid factor for the $(0001) \langle 11\text{--}20 \rangle$ slip system significantly decreased along the extrusion direction [32]. Consequently, a higher strength should be applied to activate the basal slip system, i.e. high yield strength was obtained. Therefore, the obvious enhancement of the Mg–Zn–Ca alloy after extrusion is attributed to grain refinement, high-density precipitates and strong basal texture.

Conclusions

The microstructural evolution and mechanical properties of an Mg–Zn–Ca alloy during extrusion were investigated in the present study. The following conclusions are summarised as follows.

- (1) A bimodal microstructure consisting of finely recrystallised grains and coarsely deformed grains was obtained for the as-extruded alloy.
- (2) Extrusion promoted the dynamic precipitation of fine $\text{Ca}_2\text{Mg}_6\text{Zn}_3$, part of which distributing

at grain boundaries effectively restricted grain growth and part hindered dynamic recrystallisation.

- (3) Extrusion enhanced the mechanical properties of the Mg–Zn–Ca alloy. The yield strength was increased from 42 MPa of the as-cast alloy to 285 MPa of the as-extruded alloy.
- (4) The significant improvement of mechanical properties is related to the fine microstructure, high-density precipitates and strong texture.

Disclosure statement

No potential conflict of interest was reported by the author(s).

Funding

This work was supported by National Natural Science Foundation of China [grant number 51801150]; Postdoctoral Research Foundation of China [grant number 2019M653703] and [grant number 2020T130523].

ORCID

Yuzhou Du  <http://orcid.org/0000-0003-0714-2442>

References

- [1] Zeng Z, Stanford N, Davies CHJ, et al. Magnesium extrusion alloys: a review of developments and prospects. *Int Mater Rev*. 2018;64:1–36.
- [2] He ML, Luo TJ, Zhou JX, et al. Microstructure and mechanical properties of as-cast Mg-4Zn-0.5Zr-0.2Cu-0.2Ce alloy. *Mater Sci Tech*. 2018: 1–9.
- [3] Meng S-J, Yu H, Fan S-D, et al. Recent progress and development in extrusion of rare earth Free Mg alloys: a review. *Acta Metall Sin (English Letters)*. 2019;32(2):145–168.
- [4] Wang X, Du Y, Liu D, et al. Significant improvement in mechanical properties of Mg–Zn–La alloy by minor Ca addition. *Mater Charact*. 2020;160:110130.
- [5] Yang L, Guo S, Li G-Y, et al. The microstructure, mechanical properties and corrosion behaviour of Ce-containing Mg-3Sn-1Ca alloy. *Mater Sci Tech*. 2019;35(8):946–952.
- [6] Mehranpour MS, Heydarinia A, Emamy M, et al. Enhanced mechanical properties of AZ91 magnesium alloy by inoculation and hot deformation. *Mater Sci Eng, A*. 2021;802:140667.
- [7] Khaleghi AA, Akbaripanah F, Sabbaghian M, et al. Influence of high-pressure torsion on microstructure, hardness and shear strength of AM60 magnesium alloy. *Mater Sci Eng, A*. 2021;799:140158.
- [8] Davis AE, Robson JD, Turski M. The effect of multiple precipitate types and texture on yield asymmetry in Mg–Sn–Zn(-Al–Na–Ca) alloys. *Acta Mater*. 2018;158:1–12.
- [9] Li ZT, Qiao XG, Xu C, et al. Enhanced strength by precipitate modification in wrought Mg–Al–Ca alloy with trace Mn addition. *J Alloys Compd*. 2020;836:154689.
- [10] Nakata T, Xu C, Yoshida Y, et al. Improving room-temperature stretch formability of a high-alloyed Mg–Al–Ca–Mn alloy sheet by a high-temperature solution-treatment. *Mater Sci Eng, A*. 2021;801:140399.
- [11] Jiang MG, Xu C, Nakata T, et al. High-speed extrusion of dilute Mg–Zn–Ca–Mn alloys and its effect on microstructure, texture and mechanical properties. *Mater Sci Eng, A*. 2016;678(Supplement C):329–338.
- [12] Cheng W-L, Hao M-J, Wang L-F, et al. Microstructure evolution and texture tailoring during hot compression at low temperatures of an extruded dilute Mg-0.5Sn-0.5Zn-0.5Al alloy. *Mater Sci Eng, A*. 2020;789:139606.
- [13] Yan H, Xu SW, Chen RS, et al. Activation of 10-12 twinning and slip in high ductile Mg–2.0Zn–0.8Gd rolled sheet with non-basal texture during tensile deformation at room temperature. *J Alloys Compd*. 2013;566(0):98–107.
- [14] Nakata T, Mezaki T, Xu C, et al. Improving tensile properties of dilute Mg-0.27Al-0.13Ca-0.21Mn (at.%) alloy by low temperature high speed extrusion. *J Alloys Compd*. 2015;648(0):428–437.
- [15] Nakata T, Xu C, Matsumoto Y, et al. Optimization of Mn content for high strengths in high-speed extruded Mg-0.3Al-0.3Ca (wt%) dilute alloy. *Mater Sci Eng, A*. 2016;673:443–449.
- [16] Jiang MG, Xu C, Nakata T, et al. Development of dilute Mg–Zn–Ca–Mn alloy with high performance via extrusion. *J Alloys Compd*. 2016;668:13–21.
- [17] Du YZ, Qiao XG, Zheng MY, et al. Development of high-strength, low-cost wrought Mg–2.5mass% Zn alloy through micro-alloying with Ca and La. *Mater Des*. 2015;85:549–557.
- [18] Du Y, Zheng M, Jiang B. Microstructure modification and resultant mechanical properties of Mg–6Zn–1.5Ca (wt%) alloy through hot extrusion. *J Mater Res*. 2018;33(8):1003–1010.
- [19] Du Y, Zheng M, Jiang B, et al. Deformation-Induced dynamic precipitation and resulting microstructure in a Mg–Zn–Ca alloy. *Jom-Us*. 2018;70(8):1611–1615.
- [20] Du Y, Zheng M, Jiang B. Comparison of microstructure and mechanical properties of Mg–Zn microalloyed with Ca or Ce. *Vac*. 2018;151:221–225.
- [21] Du YZ, Qiao XG, Zheng MY, et al. Effect of microalloying with Ca on the microstructure and mechanical properties of Mg-6 mass%Zn alloys. *Mater Des*. 2016;98:285–293.
- [22] Zhou L, Huang Y-D, Mao P-L, et al. Influence of composition on hot tearing in binary Mg–Zn alloys. *Int J Cast Metal Res*. 2011;24(3/4):170–176.
- [23] Zhang B, Wang Y, Geng L, et al. Effects of calcium on texture and mechanical properties of hot-extruded Mg–Zn–Ca alloys. *Mater Sci Eng, A*. 2012;539(0):56–60.
- [24] Bachmann F, Hielscher R, Schaeben H. Texture analysis with MTEX – free and open source software toolbox. *Sol St Phen*. 2010;160:63–68.
- [25] Abdel-Gawad SA, Shoeib MA. Corrosion studies and microstructure of Mg–Zn–Ca alloys for biomedical applications. *Surf Interfaces*. 2019;14:108–116.
- [26] Farahany S, Bakhsheshi-Rad HR, Idris MH, et al. In-situ thermal analysis and macroscopical characterization of Mg–xCa and Mg–0.5Ca–xZn alloy systems. *Thermochim Acta*. 2012;527(0):180–189.
- [27] Zhang XR, Sun GX, Zai W, et al. Effects of temperature and strain rate on deformation behaviors of an extruded Mg-5Zn-2.5Y-1Ce-0.5Mn alloy. *Mater Sci Eng, A*. 2021;799:140141.
- [28] Oh-ishi K, Watanabe R, Mendis CL, et al. Age-hardening response of Mg-0.3 at.%Ca alloys with different Zn contents. *Mater Sci Eng, A*. 2009;526(1-2):177–184.

- [29] Bettles CBM. *Advances in wrought magnesium alloys: fundamentals of processing, properties and applications*. Oxford: Woodhead Publishing; 2012.
- [30] Oh-ishi K, Mendis CL, Homma T, et al. Bimodally grained microstructure development during hot extrusion of Mg-2.4 Zn-0.1 Ag-0.1 Ca-0.16 Zr (at.%) alloys. *Acta Mater.* 2009;57(18):5593–5604.
- [31] Nie JF. Effects of precipitate shape and orientation on dispersion strengthening in magnesium alloys. *Scripta Mater.* 2003;48(8):1009–1015.
- [32] Xia D, Chen X, Huang G, et al. Calculation of Schmid factor in Mg alloys: Influence of stress state. *Scripta Mater.* 2019;171:31–35.